PROCEEDINGS OF THE ROYAL SOCIETY A

rspa.royalsocietypublishing.org

The sliding contact of a rigid wavy surface with a viscoelastic half-space

N. Menga[1], C. Putignano[1,2], G. Carbone[1] and G. P. Demelio[1]

[1]TriboLAB, Department of Mechanics, Mathematics and Management, Politecnico di Bari, v.le Japigia 182, Bari, Italy
[2]Imperial College, Department of Mechanical Engineering, South Kensington Campus, London, UK

GC, 0000-0002-8919-6796

Research

Cite this article: Menga N, Putignano C, Carbone G, Demelio GP. 2014 The sliding contact of a rigid wavy surface with a viscoelastic half-space. *Proc. R. Soc. A* **470**: 20140392.
http://dx.doi.org/10.1098/rspa.2014.0392

Received: 15 May 2014
Accepted: 19 June 2014

Subject Areas:
mechanical engineering, materials science

Keywords:
viscoelasticity, friction, contact mechanics

Author for correspondence:
G. Carbone
e-mail: giuseppe.carbone@poliba.it

In this paper, the contact of a rigid sinusoid sliding on a viscoelastic half-space is studied. The solution of the problem is obtained by following the path drawn by Hunter for cylindrical contacts. Results show that depending on the remote applied load, a transition from full contact conditions to partial contact may occur depending on the sliding velocity. This effect, which is not observed in smooth single asperity contacts, is related to the viscoelastic stiffening of the material and to the periodicity of the contacts. Frictional properties as well as contact area, displacement and pressure distributions are discussed in detail.

1. Introduction

Current advances in polymer technology make available a large class of new rubber and rubber-made materials for many engineering components, including either traditional products, such as tyres, belts and seals, and innovative applications, such as microelectro-mechanical systems and artificial scaffolds for biological applications. However, the smart design of such elements requires an accurate analysis of the viscoelastic material response and, in particular, of the viscoelastic dissipation, which is always entailed when using these materials. This is a crucial point in current applied mechanics research: as examples, a more efficient design of tyres or an improved sealing action of mechanical seals may have a prominent impact in terms of significant energy savings and enhanced wear resistance. This optimization research effort requires the accurate understanding of the viscoelastic properties of contact problems. The intrinsic

Royal Society Publishing

difficulty of the viscoelastic contact mechanics, whose solution is characterized by strongly dissipative phenomena [1], is marked by the huge number of different approaches, including theories [2–8] and numerical methodologies [1,9–19] developed to investigate rolling, sliding and lubricated contacts of viscoelastic materials.

Furthermore, the complexity is boosted by the roughness between the contacting surfaces. Indeed, the sliding or rolling contact between rough surfaces involves a very large number of spatial and time scales (covering more than six orders of magnitude), provoking a huge increase of computational cost and making conventional numerical techniques, including finite-element (FE) solvers, unfeasible for this type of investigations. For these reasons, specially designed numerical boundary element methodologies have been developed to address the rough contact problem [1,17,20–25]. On the other hand, different approximate analytic approaches have been proposed to deal with this type of problems, which belong mainly to two categories: (i) mean-field theories [3,5,6,26] and (ii) multi-asperity models [27–32].

In this paper, we deal with a simpler problem consisting of a viscoelastic half-space sliding in steady-state adhesionless contact with a rigid sinusoidal indenter. While the problem is interesting in itself, because it generalizes, to the case of viscoelastic contact, the Westergaard's solution [33], it also put the basis for the development of a more complicated theory of viscoelastic contact of rough profiles, because randomly rough profiles may be regarded as a sum of a multitude of sinusoid.

By following a path similar to the one proposed by Hunter [2], for the case of a rigid cylinder rolling on a viscoelastic half-space, we reformulate the problem in terms of a Fredholm integral equation of the first kind, where the logarithmic Kernel is exactly the same found for two-dimensional elastic problems [34–37], plus a couple of first-order differential equations and the corresponding boundary conditions. This formulation allows to exploit some of the solutions already known for elastic materials [34], thus leading to a strong simplification of the viscoelastic contact problem at hand.

We analyse the effect of sliding velocity and remote applied load on contact area size and shape of the deformed material and pressure distribution. Moreover, the viscoelastic frictional properties of the system are investigated. A detailed analysis is devoted to the transition from full contact to partial contact, which occurs, for load in between two limiting values, at a certain speed.

2. Formulation

We consider the problem of a sinusoidal rigid indenter in sliding contact, at constant velocity V, with a linear viscoelastic half-space. We assume no tangential stresses at the interface between the rigid indenter and solid, thus only normal stresses are present. Figure 1 shows the geometrical quantities involved in the problem. Given the wavelength λ and the amplitude h of the moving rigid sinusoidal indenter, of shape $y(x,t) = h\cos[2\pi(x - Vt)/\lambda]$, we define the mean separation s as the distance between the mean lines of the rigid indenter and of the deformed viscoelastic body. The penetration of the sinusoidal indenter into the viscoelastic half-space is then defined as $\Delta = h - s$. The quantity $v(x)$ is the profile measured from the mean line of the deformed viscoelastic body.

Now, assuming $h/\lambda \ll 1$, the linearity of the viscoelastic material allows us to relate the time-dependent displacement field $v(x,t)$ with the time-dependent normal stress distribution $\sigma(x,t)$ through the constitutive equation

$$v(x,t) = \int_{-\infty}^{t} \mathrm{d}z \int_{-\infty}^{+\infty} \mathrm{d}\xi\, \mathcal{G}(x-\xi, t-z)\dot{\sigma}(\xi, z), \tag{2.1}$$

where $\dot{\sigma}(x,t)$ is the time derivative of normal stress distribution at the interface, $\mathcal{G}(x,t)$ is Green's function. Invoking the elastic–viscoelastic correspondence principle [38] enables us to factorize

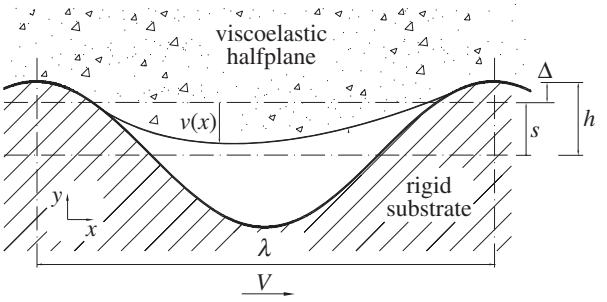

Figure 1. The geometrical scheme of the contact problem.

Green's function as $\mathcal{G}(x,t) = G(x)J(t)$, where

$$G(x) = -\frac{2(1-\nu^2)}{\pi}\log\left[2\left|\sin\left(\frac{kx}{2}\right)\right|\right] \tag{2.2}$$

is the purely elastic Green's function obtained in [34–37] with $k = 2\pi/\lambda$, whereas $J(t)$ is the viscoelastic creep function. By adopting the linear standard model formulation for a one relaxation time viscoelastic material, the creep function takes the following form

$$J(t) = H(t)\left[\frac{1}{E_0} - \frac{1}{E_1}\exp\left(\frac{-t}{\tau}\right)\right], \tag{2.3}$$

where $H(t)$ is the Heaviside step function, and E_0 is the low frequency elastic modulus. Because we are interested in determining the long-time response of the system, when any information about the initial state has been completely lost, we can write that $v(x,t) = v(x - Vt)$ and $\sigma(x,t) = \sigma(x - Vt)$. Therefore, using the substitution $(x - Vt) \to x$, the problem can be rephrased as [1,17,18]:

$$v(x) = \int \mathrm{d}\xi\, \Phi_V(x-\xi)\sigma(\xi), \tag{2.4}$$

where $\Phi_V(x)$ is the new Green's function for steady-state sliding contacts, which parametrically depends on the constant sliding speed V

$$\Phi_V(x) = J(0^+)G(x) + \int_{0^+}^{+\infty} \mathrm{d}z\, G(x+Vz)\dot{J}(z). \tag{2.5}$$

Using equations (2.2) and (2.3), and recalling that $J(0^+) = 1/E_0 - 1/E_1 = 1/E_\infty$, where E_∞ is the high-frequency elastic modulus of the material, equation (2.4) becomes

$$\begin{aligned} -v(x) = {} & \frac{1}{E_\infty}\frac{2(1-\nu^2)}{\pi}\int_{-\lambda/2}^{\lambda/2}\mathrm{d}\xi\,\log\left|2\sin\left(\frac{k(x-\xi)}{2}\right)\right|\sigma(\xi) \\ & + \frac{1}{E_1}\frac{2(1-\nu^2)}{\pi}\int_{0^+}^{+\infty}\mathrm{d}z\exp(-z)\int_{-\lambda/2}^{\lambda/2}\mathrm{d}\xi\,\sigma(\xi)\log\left|2\sin\left(\frac{k(x-\xi+v\tau z)}{2}\right)\right| \end{aligned} \tag{2.6}$$

Now, using the same approach proposed by Hunter [2], equation (2.6) takes the form

$$q(x) = -\frac{1}{E_0}\frac{2(1-\nu^2)}{\pi}\int_{-\lambda/2}^{\lambda/2}\mathrm{d}\xi\; p(\xi)\log\left|2\sin\left(\frac{k(x-\xi)}{2}\right)\right|, \tag{2.7}$$

where

$$\left.\begin{aligned} p(x) &= \sigma(x) - v\tau\frac{E_0}{E_\infty}\frac{\mathrm{d}\sigma(x)}{\mathrm{d}x} \\ \text{and}\qquad q(x) &= v(x) - V\tau\frac{\mathrm{d}v(x)}{\mathrm{d}x}. \end{aligned}\right\} \tag{2.8}$$

Interestingly, equation (2.7) looks exactly the same as in the case of periodic two-dimensional elastic contacts [34–37], the only differences being that, this time, the stress distribution is replaced

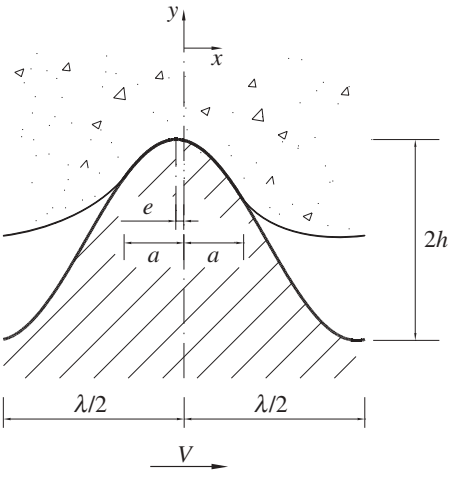

Figure 2. The shape of contact. The quantity e indicates the contact area eccentricity.

by $p(x)$ and the elastic displacement by $q(x)$. Therefore, the analytical elastic solution obtained in [34] can be successfully exploited to solve the problem at hand. Note that, during the sliding at finite speed V, because of the viscoelastic response of the material, the contact area, of size $2a$ (figure 2), will show a certain degree of asymmetry, quantified by the eccentricity parameter e (figure 2). Thus, recalling that in the contact domain $\Omega = [-a, a]$ the elastic displacement is

$$v(x) = h\cos(kx + ke) - s; \quad x \in \Omega.$$

Equation (2.7) can be split into the following two equations

$$h_1\cos(kx + ke_1) - s = -\frac{1}{E_0}\frac{2(1-\nu^2)}{\pi}\int_{-a}^{a} \mathrm{d}\xi p(\xi)\log\left|2\sin\left(\frac{k(x-\xi)}{2}\right)\right|; \quad x \in \Omega \tag{2.9}$$

and

$$q(x) = -\frac{1}{E_0}\frac{2(1-\nu^2)}{\pi}\int_{-a}^{a} \mathrm{d}\xi\ p(\xi)\log\left|2\sin\left(\frac{k(x-\xi)}{2}\right)\right|; \quad x \notin \Omega \tag{2.10}$$

where we have defined the following quantities

$$\left.\begin{aligned} h_1 &= h\sqrt{1+(V\tau k)^2} \\ e_1 &= e + \alpha \\ \cos(k\alpha) &= \frac{1}{\sqrt{1+(V\tau k)^2}} \\ \text{and} \qquad \sin(k\alpha) &= -\frac{V\tau k}{\sqrt{1+(V\tau k)^2}}. \end{aligned}\right\} \tag{2.11}$$

As shown in reference [34], equations (2.9) and (2.10) can be analytically solved (see appendix A), and allow to calculate, for any given sliding velocity V, the quantities $q(x; a, e, p_\infty)$ and $p(x; a, e, p_\infty)$ as functions of the parameters a, e, and the remote applied pressure $p_\infty = -\lambda^{-1}\int_\Omega \mathrm{d}x\sigma(x) = \lambda^{-1}\int_\Omega \mathrm{d}x p(x)$. However, given the applied pressure p_∞, the size $2a$ of the

contact area and the eccentricity e are not independent quantities and must be determined as a part of the solution. To accomplish this purpose, once known $q(x;a,e,p_\infty)$ and $p(x;a,e,p_\infty)$ from equations (2.9) and (2.10), we need to solve equations (2.8) with the four boundary conditions

$$\left.\begin{aligned}\sigma(a)&=0\\ \sigma(-a)&=0\end{aligned}\right\} \tag{2.12}$$

and

$$\left.\begin{aligned}v(a)&=h\cos(ka+ke)-s\\ v(-a)&=h\cos(ka-ke)-s.\end{aligned}\right\} \tag{2.13}$$

Equations (2.12) and (2.13) enable us to determine the two constants of integration of equations (2.8), and to write the following additional closure equations

$$\int_{-a}^{a} p(x;a,e,p_\infty)\exp\left(-\frac{E_\infty}{E_0}\frac{x}{V\tau}\right)\mathrm{d}x=0 \tag{2.14}$$

and

$$\frac{1}{V\tau k}\frac{1-\nu^2}{E_0}\int_a^{\lambda-a} q(x;a,e,p_\infty)\exp\left(-\frac{x}{V\tau}\right)\mathrm{d}x=kh\left[\cos(ka+ke)\exp\left(-\frac{a}{V\tau}\right)-\cos(ka-ke)\exp\left(-\frac{\lambda-a}{V\tau}\right)\right] \tag{2.15}$$

Equations (2.14) and (2.15) finally allow to calculate the semi-contact width a and the contact eccentricity e as a function of the remote applied pressure p_∞.

3. Results

Here, we discuss the main peculiarities of the viscoelastic problem under investigation in terms of contact area, penetration and viscoelastic friction. We also show how these quantities depend on the sliding velocity V. In the calculations, we use $E_\infty/E_0=3$ and define the reference sliding velocity $V_0=(\tau k)^{-1}$, and the dimensionless remote applied pressure $\tilde{p}_\infty=p_\infty(1-\nu^2)/E_0$.

Figure 3*a* shows the shape of the deformed profile given the applied load $\tilde{p}_\infty=0.3$. We observe that at very small or very high sliding velocity V, the Westergaard's elastic solution is recovered [33,34,36]. This is because the viscoelastic material shows an elastic behaviour at very small and very high frequencies, with two different values of the elastic modulus: E_0 and E_∞, respectively. In particular, at constant load (figure 3*a*) and extremely low sliding velocity, the system behaves as a soft elastic material, with elastic modulus E_0, and no viscoelastic dissipation takes places, making the interfacial stress and displacement distributions perfectly symmetric. As V is increased, the material stiffens and, given the same applied load, it penetrates less into the substrate. In such conditions, the hysteretic behaviour of the viscoelastic materials leads to a clear asymmetry of the contact region, characterized by a marked shrinkage at the trailing edge of the contact. At very high sliding velocity, the material behaves again elastically but it is much stiffer, with elastic modulus E_∞. In this case, the symmetry of stress and displacement distributions is again recovered. This time, given the same applied load $\tilde{p}_\infty$, the penetration is much smaller because of the significantly higher stiffness, i.e. $E_\infty>E_0$. On the other hand, if we keep constant the penetration Δ (figure 3*b*), the displacement fields, obtained in these two limiting elastic cases, are exactly the same. This is not surprising, because dimensional arguments (as confirmed by the Westergaard's elastic solution) lead to the conclusion that the relation between the penetration Δ, the contact area $2a$, the amplitude h of the sinusoidal rigid substrate and its wavelength λ, cannot involve the remote load p_∞. Figure 4, shows the penetration Δ as a function of the remote load p_∞ for different values of the ratio V/V_0. Of course, Δ increases with the applied pressure p_∞, however, as qualitatively shown before, at fixed p_∞ an increase of V causes a significant reduction of the penetration Δ. Similarly, in figure 5, the dependence of the semi-contact area a on the dimensionless load $\tilde{p}_\infty$ is shown for different values of the ratio V/V_0. As expected, because of

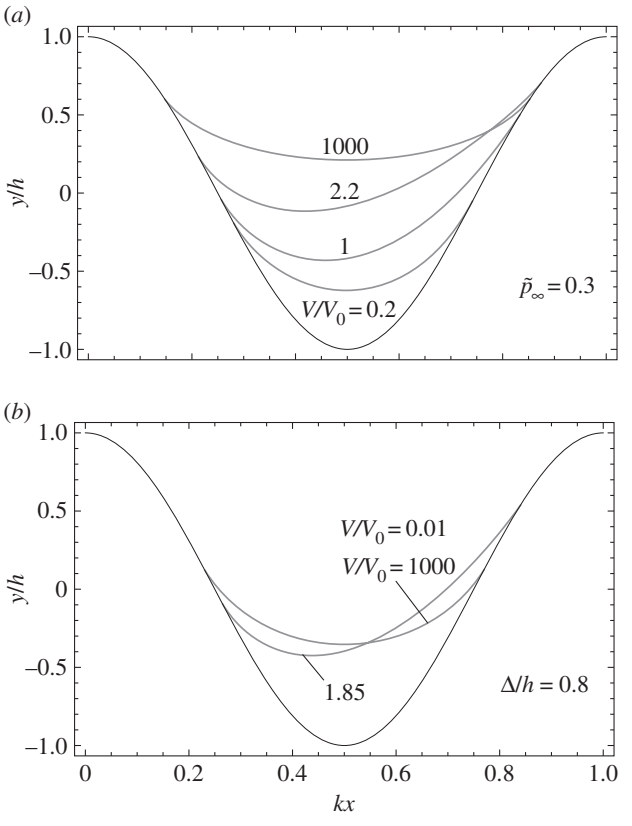

Figure 3. The deformed profile for different values of the ratio V/V_0: at fixed load $\tilde{p}_\infty = 0.3$, (*a*); at fixed penetration $\Delta/h = 0.8$ (*b*).

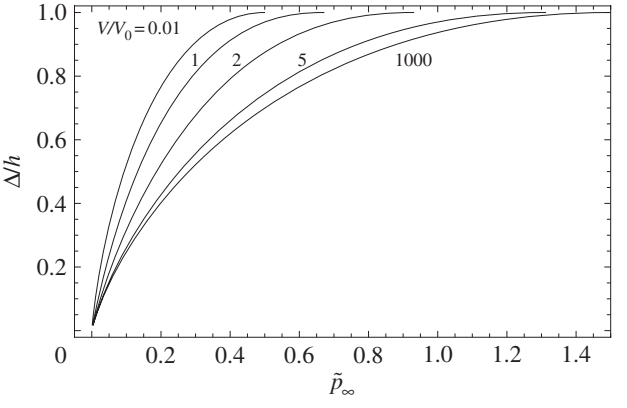

Figure 4. The dimensionless penetration Δ/h as a function of the dimensionless load $\tilde{p}_\infty$ for different V/V_0.

velocity induced viscoelastic stiffening, at fixed applied load p_∞, the semi-contact area a decreases as the sliding velocity is increased. On the other hand, in figure 6, we plot the semi-contact area a as a function of the penetration Δ. We note that, at extremely slow and extremely high velocities the curves a versus Δ perfectly overlap to each other. Different is the case of intermediate sliding velocity, when viscoelasticity plays a significant role causing the a versus Δ curve to deviate from the perfectly elastic cases. This is even more clear in figure 7 where, given the value of

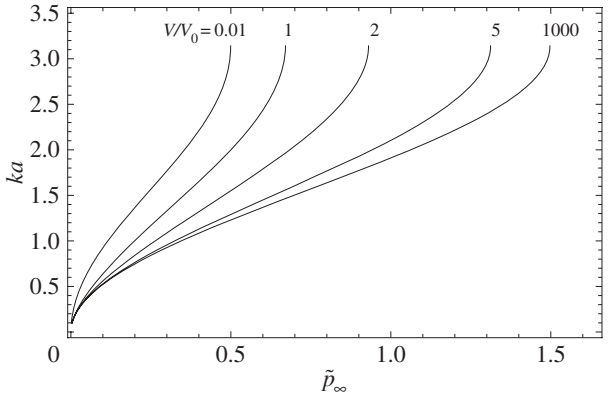

Figure 5. The dimensionless area ka as a function of the dimensionless load $\tilde{p}_\infty$ for different V/V_0.

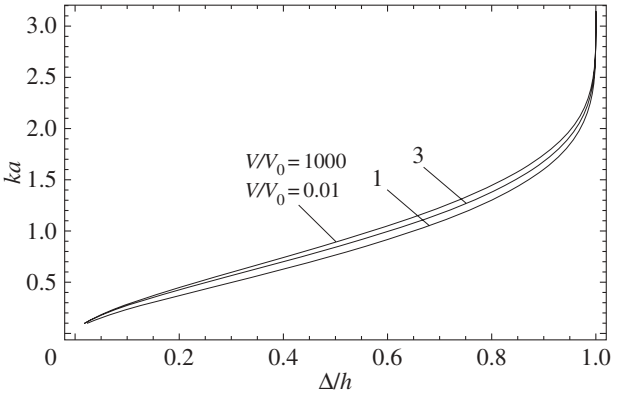

Figure 6. The dimensionless area ka as a function of the dimensionless penetration Δ/h for different V/V_0.

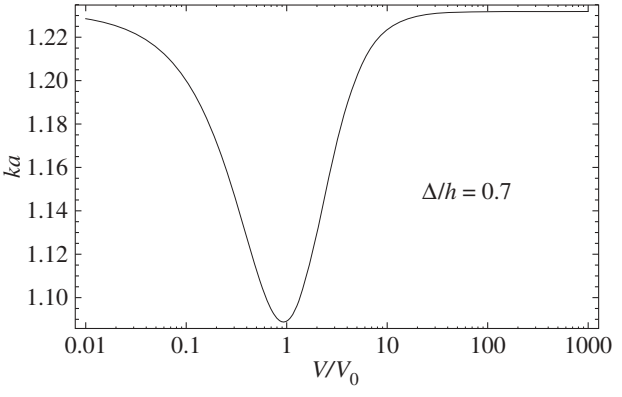

Figure 7. The dimensionless area ka as a function of the ratio V/V_0 for a fixed dimensionless penetration Δ/h.

penetration Δ, the contact area first decreases as the sliding velocity V is increased, then reaches a minimum value corresponding to a sliding velocity $V \approx V_0$, at which viscoelastic effects are maximized, and then increases again towards the high-speed elastic solution. This behaviour is expected because, at intermediate velocity, the effect of internal viscous losses is mainly to

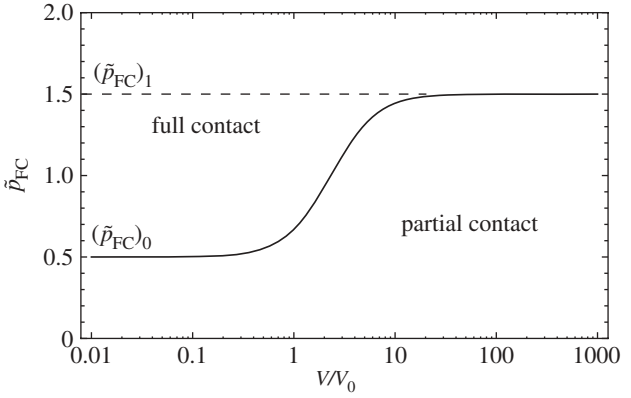

Figure 8. The minimum dimensionless load $\tilde{p}_{FC}$ needed to ensure full contact. $\tilde{p}_{FC}$ ranges from the value $(\tilde{p}_{FC})_0$, reached at extremely low velocities, to the value $(\tilde{p}_{FC})_1$, corresponding to extremely high velocities.

strongly reduce the contact pressure at the trailing edge, thus leading to a reduction of the contact area size.

In appendix B, the minimum value p_{FC} of the remote applied load which causes the system to snap in full contact is calculated (see also figure 8). Of course, p_{FC} is minimal in the limit of extremely small velocities [$p_{FC} = (p_{FC})_0$], and it monotonously increases until its maximum value [$p_{FC} = (p_{FC})_1$] is reached at very large velocities. In our case, we calculated $(\tilde{p}_{FC})_0 = 0.5$ and $(\tilde{p}_{FC})_1 = 1.5$, which is in agreement with $E_\infty/E_0 = 3$. Therefore, for $(p_{FC})_0 < p_\infty < (p_{FC})_1$, it happens that the system experiences full contact at sliding velocities below a certain threshold V_{th}, and then undergoes a transition to partial contact conditions because of the material stiffening. This particular behaviour cannot be observed in smooth single asperity contacts. It is peculiar of viscoelastic periodic contacts, where viscoelastic interaction between asperities in contact plays a fundamental role. For each given value of the remote pressure $\tilde{p}_\infty$, the threshold value V_{th} can be calculated by solving the equation

$$\frac{|E(kV_{th})|}{E_0} = \frac{2}{hk}\tilde{p}_\infty,$$

where $E(\omega)$ is the complex viscoelastic modulus defined as $E(\omega)^{-1} = i\omega J(\omega)$, with $J(\omega) = \int dt J(t) \exp(-i\omega t)$.

Figure 9 shows, for $V < V_{th}$, the system in full contact (i.e. $ka = \pi$). However, as soon as the sliding velocity exceeds the value, V_{th} partial contact conditions are established, and the contact area continuously shrinks as the sliding velocity Va is increased.

The transition from full contact to partial contact affects the eccentricity e of the contact area and the eccentricity $\hat{e}$ of the pressure distribution (figure 10). The latter is defined as

$$\hat{e} = \frac{\int_\Omega dx x p(x)}{\int_\Omega dx p(x)}.$$

We observe that in full contact, because of linearity, both displacement and pressure distributions are sinusoidal. In this case, the quantity e can no longer be defined, whereas $\hat{e}$ has a clear physical meaning: it represents the spatial phase shift between the sinusoidal pressure distribution and the sinusoidal displacement field. This phase shift leads to non-zero friction force (see appendix B).

For remote pressure values $(p_{FC})_0 < p_\infty < (p_{FC})_1$, see figure 11, the pressure eccentricity $\hat{e}$ follows a bell-shaped curve, whereas the contact area eccentricity e, which can be defined only in partial contact conditions, i.e. for $V > V_{th}$, is always smaller than $\hat{e}$, except at $V = V_{th}$ when the two quantities take the same value.

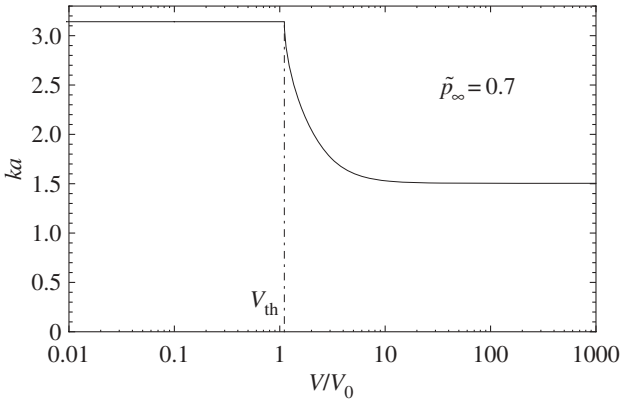

Figure 9. The dimensionless contact area as a function of the ratio V/V_0 for the dimensionless load $(\tilde{p}_{FC})_0 < \tilde{p}_\infty = 0.7 < (\tilde{p}_{FC})_1$.

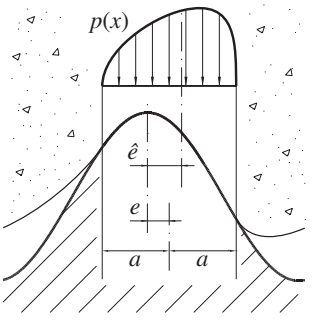

Figure 10. The parameters e and $\hat{e}$ are respectively the eccentricity of the contact area and the eccentricity of the pressure distribution.

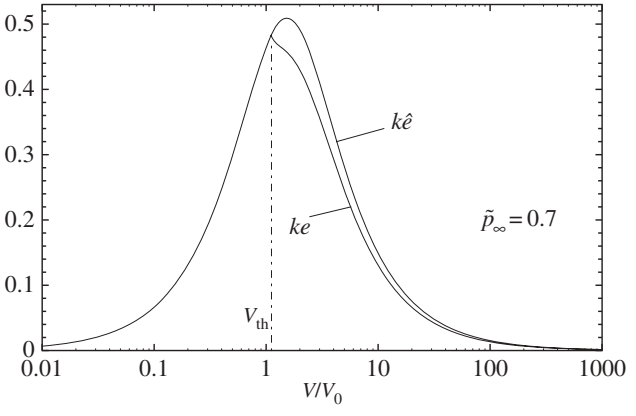

Figure 11. The dimensionless eccentricity $k\hat{e}$ of the pressure distribution and the dimensionless eccentricity ke of the contact area as functions of the ratio V/V_0 for the fixed dimensionless normal load $(\tilde{p}_{FC})_0 < \tilde{p}_\infty = 0.7 < (\tilde{p}_{FC})_1$. Interestingly, at the threshold sliding velocity value V_{th}, below which full contact is established, both ke and $k\hat{e}$ coincide. For $V < V_{th}$, the quantity ke can no longer be defined.

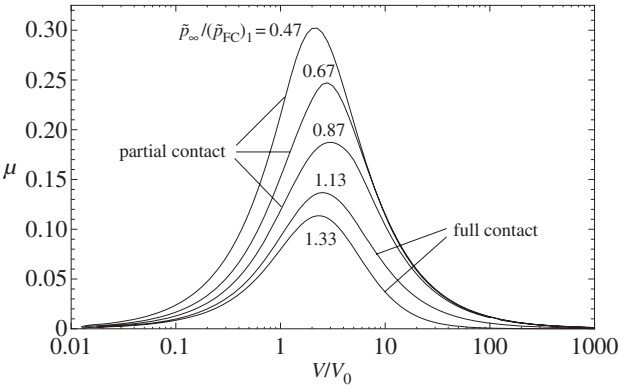

Figure 12. The friction coefficient μ as a function of the ratio V/V_0 for different values of the ratio $p_\infty/(p_{FC})_1$.

We also calculated the mean frictional stress

$$\tau_f = \frac{1}{\lambda}\int_\Omega \mathrm{d}x\sigma(x)\frac{\partial v}{\partial x} \tag{3.1}$$

and the coefficient of friction as $\mu = \tau_f/p_\infty$, the latter is represented in figure 12 as a function of the sliding velocity V, for different values of the dimensionless remote load $\tilde{p}_\infty$. As expected, μ is described by bell-shaped curves, with almost no friction in the limiting cases of extremely small and extremely high sliding velocities, when the material behaves elastically. It is noteworthy to observe that, when the system is in full contact conditions, a further increase of the load leads to a decrease of the friction coefficient μ. This is expected, because, once full contact is reached, τ_f no longer changes with the normal load p_∞, and therefore the friction coefficient μ, defined above, must decrease as p_∞ is increased (see appendix B).

4. Conclusion

We have studied the sliding contact of a rigid sinusoid over a viscoelastic half-space. We reformulate the problem into an equivalent elastic contact by means of ad hoc transformations of displacement and pressure distributions. This allows us to exploit existing elastic solutions of sinusoidal contact [34]. Results show that, depending on the remote applied load, particular conditions may occur which cause the contact to undergo a transition from full contact to partial contact as the sliding speed is increased. This effect cannot be observed in smooth single asperity contacts, as it is strongly related to the viscoelastic interaction between asperities in contact which necessarily occurs in periodic contacts. We also investigate how the shape of the contact, the contact area and the penetration, as well as the coefficient of friction are affected by the sliding speed and the remote load.

Funding statement. The authors thank the Italian Ministry of Education, University and Research for supporting the research activity within the projects PON01-02238 and PON02 00576-3333604. C.P. also gratefully acknowledges the support of Marie Curie IEF project SOFT-MECH (grant no. 622632).

Appendix A. The elastic contact solution

The viscoelastic solution, presented in the paper, was obtained by using the elastic-viscoelastic correspondence principle [38] which allowed us to exploit the results found, for the elastic case, by one of the authors in [34], where the adhesive non-symmetric contact between an elastic half-space and a rigid sinusoidal substrate has been studied. Here, we briefly summarize the main results obtained in [34]. The main problem is to solve the integral equation (2.9) and calculate the

integral equation (2.10), given the contact domain $\Omega =]-a, a[$. The aforementioned problem can be solved by invoking the superposition principle and dual series approach [39]. The solution is, then, the sum of an asymmetric solution, denoted with the subscript 1 and a symmetric one, denoted with the subscript 2.

$$\left.\begin{aligned} q(x) &= q_1(x) + q_2(x) \\ \text{and} \quad p(x) &= p_1(x) + p_2(x) \end{aligned}\right\}, \tag{A 1}$$

where

$$p_1(x,0) = \frac{Ekh\sin(ke)}{4(1-\nu^2)}\sin(kx)\chi(x)\left[g(kx,ka) + \frac{1}{g(kx,ka)}\right] \tag{A 2}$$

and

$$q_1(x,0) = -h\sin(ke)\sin(kx)\{1-[1-\chi(x)]f(kx,ka)\} \tag{A 3}$$

with

$$g(kx,ka) = \sqrt{1 - \frac{\cos^2(ka/2)}{\cos^2(kx/2)}} \tag{A 4}$$

and

$$f(kx,ka) = \sqrt{1 - \frac{\sin^2(ka/2)}{\sin^2(kx/2)}} \tag{A 5}$$

and $\chi(x)$ is the characteristic function of the contact domain: $\chi(x) = 1$ for $x \in \Omega$ and $\chi(x) = 0$ otherwise.

The symmetric solution is found by superposing two simpler problems. The first one deals with the non-adhesive contact of an elastic half-space indented by a sinusoidal surface of amplitude $h\cos(ke)$, which has been solved by Westergaard [33], where the asymptotic pressure $p_{W\infty}$ is introduced. The second term corresponds to an infinite row of collinear cracks [39,40] of width $\lambda - 2a$, under an apparent asymptotic tensile load $\sigma_{K\infty} = p_{W\infty} - p_\infty > 0$. Under these premises, the solution is

$$p_2(x,0) = p_W(x,0) + p_K(x,0) \tag{A 6}$$

and

$$q_2(x,0) = q_W(x,0) + q_K(x,0), \tag{A 7}$$

where

$$p_W(x,0) = -2p_{W\infty}\chi(x)\frac{\cos^2(kx/2)}{\sin^2(ka/2)}\sqrt{1 - \frac{\cos^2(ka/2)}{\cos^2(kx/2)}} \tag{A 8}$$

$$p_{W\infty} = \frac{E}{2(1-\nu^2)}kh\cos(ke)\sin^2\left(\frac{ka}{2}\right) \tag{A 9}$$

and

$$p_K(x,0) = \sigma_{K\infty}\chi(x)\left[1 - \frac{\cos^2(ka/2)}{\cos^2(kx/2)}\right]^{-1/2}, \tag{A 10}$$

and

$$\begin{aligned} q_W(x,0) = {} & h\cos(ke)\cos(kx) + 2h\cos(ke)[1-\chi(x)] \\ & \times \left\{\sin^2\frac{kx}{2}f(kx,ka) - \sin^2\frac{ka}{2}\log\left(\frac{\sin(kx/2)}{\sin(ka/2)}[1+f(kx,ka)]\right)\right\} \end{aligned} \tag{A 11}$$

and

$$q_K(x,0) = \frac{2\sigma_{K\infty}}{k}[1-\chi(x)]\frac{2(1-\nu^2)}{E}\log\left\{\frac{\sin(kx/2)}{\sin(ka/2)}[1+f(kx,ka)]\right\} \tag{A 12}$$

Appendix B. Friction in full contact conditions

In full contact, one may easily determine the solution of the viscoelastic contact problem taking into consideration that, because of linearity, the pressure distribution will be sinusoidal as well, but, because of internal dissipation, pressure and displacement distributions will have different phases. In Fourier space, the relation between the stress σ and the displacement u can be written as [5,35,41]

$$\sigma(k,\omega) = M^{-1}(k,\omega)u(k) \tag{B 1}$$

where

$$\sigma(k,\omega) = \int \mathrm{d}x\,\mathrm{d}t\sigma(x,t)\,\mathrm{e}^{-\mathrm{i}(kx-\omega t)}$$

$$u(k,\omega) = \int \mathrm{d}x\,\mathrm{d}t u(x,t)\,\mathrm{e}^{-\mathrm{i}(kx-\omega t)}$$

and

$$M(k,\omega) = -\frac{2[1-\nu^2]}{E(\omega)|k|} \tag{B 2}$$

Now, recalling that the viscoelastic slab is sliding at constant velocity V on a rigid surface, we can write $\sigma(x,t) = \sigma(x-Vt)$ and $u(x,t) = u(x-Vt)$. In Fourier space, we obtain

$$\sigma(k,\omega) = \sigma(k)\delta(\omega - kV)$$

$$u(k,\omega) = u(k)\delta(\omega - kV),$$

where

$$\sigma(k) = \int \mathrm{d}x\sigma(x,t)\,\mathrm{e}^{-\mathrm{i}kx} \tag{B 3}$$

and

$$u(k) = \int \mathrm{d}x\, u(x,t)\,\mathrm{e}^{-\mathrm{i}kx} \tag{B 4}$$

Equation (B 1) can be conveniently rephrased as

$$\sigma(k) = M^{-1}(k,kV)u(k) \tag{B 5}$$

Equation (B 5) simply states that, for the case we are investigating where the viscoelastic body is sliding in contact with a sinusoidal substrate $u(x) = h\cos(kx)$, the interfacial stress distribution is given by

$$\sigma(x) = \sigma_{\max}\cos(kx+\varphi), \tag{B 6}$$

where

$$\left.\begin{aligned}\sigma_{\max} &= h|M^{-1}(k,kV)|\\ \text{and}\qquad \varphi &= \arg[|M^{-1}(k,kV)|]\end{aligned}\right\} \tag{B 7}$$

The friction force, $F_T = \int \mathrm{d}x\sigma(x,kV)u'(x)$, becomes

$$F_T = \pi h^2|M^{-1}(k,kV)|\sin(\varphi(kV)) = \pi h^2\,\mathrm{Im}[M^{-1}(k,kV)] \tag{B 8}$$

which, as expected for full contact conditions, does not depend on the normal load.

References

1. Carbone G, Putignano C. 2013 A novel methodology to predict sliding/rolling friction in viscoelastic materials: theory and experiments. *J. Mech. Phys. Solids* **61**, 1822–1834. (doi:10.1016/j.jmps.2013.03.005)
2. Hunter SC. 1961 The rolling contact of a rigid cylinder with a viscoelastic half space. *Trans. ASME, Ser. E, J. Appl. Mech.* **28**, 611–617. (doi:10.1115/1.3641792)
3. Persson BNJ. 2010 Rolling friction for hard cylinder and sphere on viscoelastic solid. *Eur. Phys. J. E* **33**, 327–333. (doi:10.1140/epje/i2010-10678-y)

4. Panek C, Kalker JJ. 1980 Three-dimensional contact of a rigid roller traversing a viscoelastic half space. *J. Inst. Appl. Math.* **26**, 299–313. (doi:10.1093/imamat/26.3.299)
5. Persson BNJ. 2001 Theory of rubber friction and contact mechanics. *J. Chem. Phys.* **115**, 3840–3861. (doi:10.1063/1.1388626)
6. Persson BNJ. 2006 Rubber friction: role of the flash temperature. *J. Phys. Condensed Matter* **18**, 7789–7823. (doi:10.1088/0953-8984/18/32/025)
7. Scaraggi M, Carbone G, Persson BNJ, Dini D. 2011 Lubrication in soft rough contacts: a novel homogenized approach. Part I: theory. *Soft Matter* **7**, 10 395–10 406. (doi:10.1039/C1SM05128H)
8. Campana C, Persson BNJ, Mueser MH. 2011 Transverse and normal interfacial stiffness of solids with randomly rough surfaces. *J. Phys. Condensed Matter* **23**, 085001. (doi:10.1088/0953-8984/23/8/085001)
9. Le Tallec P, Rahler C. 1994 Numerical models of steady rolling for non-linear viscoelastic structures in finite deformations. *Int. J. Numer. Methods Eng.* **37**, 1159–1186. (doi:10.1002/nme.1620370705)
10. Vollebregt EAH. User guide for CONTACT, J.J. Kalker's variational contact model. Technical Report no. TR09-03, version 1.18. Delft, The Netherlands: VORtech Computing, the Scientific Software Engineers.
11. Padovan J, Paramadilok O. 1984 Transient and steady state viscoelastic rolling contact. *Comput. Struct.* **20**, 545–553. (doi:10.1016/0045-7949(85)90102-6)
12. Padovan J. 1987 Finite element analysis of steady and transiently moving/rolling nonlinear viscoelastic structure-I. Theory. *Comput. Struct.* **27**, 249–257. (doi:10.1016/0045-7949(87)90093-9)
13. Padovan J, Kazempour A, Tabaddor F, Brockman B. 1992 Alternative formulations of rolling contact problems. *Finite Elements Anal. Des.* **11**, 275–284. (doi:10.1016/0168-874X(92)90010-A)
14. Nackenhorst U. 2004 The ALE-formulation of bodies in rolling contact theoretical foundations and finite element approach. *Comput. Method Appl. M* **193**, 4299–4322. (doi:10.1016/j.cma.2004.01.033)
15. Nasdala L, Kaliske M, Becker A, Rothert H. 1998 An efficient viscoelastic formulation for steady-state rolling structures. *Comput. Mech.* **22**, 395–403. (doi:10.1007/s004660050371)
16. Putignano C, Reddyhoff T, Carbone G, Dini D. 2013 Experimental investigation of viscoelastic rolling contacts: a comparison with theory. *Tribol. Lett.* **51**, 105–113. (doi:10.1007/s11249-013-0151-9)
17. Carbone G, Putignano C. 2014 Rough viscoelastic sliding contact: theory and experiments. *Phys. Rev. E* **89**, 032408. (doi:10.1103/PhysRevE.89.032408)
18. Putignano C, Le Rouzic J, Reddyhoff T, Carbone G, Dini D. 2013 A theoretical and experimental study of viscoelastic rolling contacts incorporating thermal effects. *Proc. Inst. Mech. Eng. Part J: J. Eng. Tribol.* (doi:10.1177/1350650114530681)
19. Campana C, Mueser MH, Robbins MO. 2008 Elastic contact between self-affine surfaces: comparison of numerical stress and contact correlation functions with analytic predictions. *J. Phys. Condensed Matter* **20**, 354013. (doi:10.1088/0953-8984/20/35/354013)
20. Putignano C, Afferrante L, Carbone G, Demelio G. 2012 A new efficient numerical method for contact mechanics of rough surfaces. *Int. J. Solids Struct.* **49**, 338–343. (doi:10.1016/j.ijsolstr.2011.10.009)
21. Putignano C, Afferrante L, Carbone G, Demelio G. 2012 The influence of the statistical properties of self-affine surfaces in elastic contact: a numerical investigation. *J. Mech. Phys. Solids*. **60**, 973–982. (doi:10.1016/j.jmps.2012.01.006)
22. Putignano C, Afferrante L, Carbone G, Demelio GP. 2013 A multiscale analysis of elastic contacts and percolation threshold for numerically generated and real rough surfaces. *Tribol. Int.* **64**, 148–154. (doi:10.1016/j.triboint.2013.03.010)
23. Scaraggi M, Putignano C, Carbone G. 2013 Elastic contact of rough surfaces: a simple criterion to make 2D isotropic roughness equivalent to 1D one. *Wear* **297**, 811–817. (doi:10.1016/j.wear.2012.10.004)
24. Campana C, Muser MH. 2007 Contact mechanics of real vs. randomly rough surfaces: a Green's function molecular dynamics study. *Europhys. Lett.* **77**, 38005. (doi:10.1209/0295-5075/77/38005)
25. Pastewka L, Robbins MO. 2014 When are rough surfaces sticky? *Proc. Natl Acad. Sci. USA* **111**, 3298–3303. (doi:10.1073/pnas.1320846111)

26. Ciavarella M, Demelio G, Barber JR, Jang YH. 2000 Linear elastic contact of the Weierstrass profile. *Proc. R. Soc. Lond. A* **456**, 387–405. (doi:10.1098/rspa.2000.0522)
27. Greenwood JA, Williamson JBP. 1966 Contact of nominally flat surfaces. *Proc. R. Soc. Lond. A* **295**, 300–319. (doi:10.1098/rspa.1966.0242)
28. Greenwood JA. 2006 A simplified elliptic model of rough surface contact. *Wear* **261**, 191–200. (doi:10.1016/j.wear.2005.09.031)
29. Greenwood JA, Putignano C, Ciavarella M. 2011 A Greenwood & Williamson theory for line contact. *Wear* **270**, 332–334. (doi:10.1016/j.wear.2010.11.002)
30. Bush AW, Gibson RD, Thomas TR. 1975 The elastic contact of a rough surface. *Wear* **35**, 87–111. (doi:10.1016/0043-1648(75)90145-3)
31. Carbone G, Bottiglione F. 2008 Asperity contact theories: do they predict linearity between contact area and load? *J. Mech. Phys. Solids* **56**, 2555–2572. (doi:10.1016/j.jmps.2008.03.011)
32. Carbone G. 2009 A slightly corrected Greenwood and Williamson model predicts asymptotic linearity between contact area and load. *J. Mech. Phys. Solids* **57**, 1093–1102. (doi:10.1016/j.jmps.2009.03.004)
33. Westergaard HM. 1939 Bearing pressures and cracks. *Trans. ASME J. Appl. Mech.* **6**, 49–53.
34. Carbone G, Mangialardi L. 2004 Adhesion and friction of an elastic half-space in contact with a slightly wavy rigid surface. *J. Mech. Phys. Solids* **52**, 1267–1287. (doi:10.1016/j.jmps.2003.12.001)
35. Carbone G, Mangialardi L. 2008 Analysis of adhesive contact of confined layers by using a Green's function approach. *J. Mech. Phys. Solids* **56**, 684–706. (doi:10.1016/j.jmps.2007.05.009)
36. Carbone G, Scaraggi M, Tartaglino U. 2009 Adhesive contact of rough surfaces: comparison between numerical calculations and analytical theories. *Eur. Phys. J. E, Soft Matter* **30**, 65–74. (doi:10.1140/epje/i2009-10508-5)
37. Carbone G, Pierro E. 2012 The influence of the fractal dimension of rough profiles on the adhesive contact of elastic materials. *J. Adhes. Sci. Technol.* **26**, 2555–2570. (doi:10.1163/156856111X623140).
38. Christensen RM. 1982 *Theory of viscoelasticity*. New York, NY: Academic Press.
39. Sneddon IN. 1966 *Mixed boundary value problems in potential theory*. Amsterdam, The Netherlands: North-Holland.
40. Koiter WT. 1959 An infinite row of collinear cracks in an infinite elastic sheet. *Ing. Arch.* **28**, 165. (doi:10.1007/BF00536108)
41. Carbone G, Lorenz B, Persson BNJ, Wohlers A. 2009 Contact mechanics and rubber friction for randomly rough surfaces with anisotropic statistical properties. *Eur. Phys. J. E, Soft Matter* **29**, 275–284. (doi:10.1140/epje/i2009-10484-8)